Macromolecules

pubs.acs.org/Macromolecules Article

Improved Exciton Bandwidth and Edge-On Oriented Ordering of Donor−Acceptor Copolymer Thin Films

Saugata Roy, Md Saifuddin, Subhankar Mandal, Jasper R. Plaisier, and Satyajit Hazra*

Cite This: *Macromolecules* 2023, 56, 7065−7077 Read Online

ACCESS | Metrics & More | Article Recommendations | Supporting Information

ABSTRACT: Donor−acceptor (D−A) copolymers having strong intermolecular interaction-induced aggregation can exhibit far higher mobilities compared to the homopolymers and, thus, are preferred as active layers for optoelectronic devices. However, the actual performances of such devices strongly depend on the conjugation length, i.e., backbone planarity or exciton bandwidth (EB) and edge-on oriented (EO) ordering of the copolymer aggregates and, thus, their understanding and improvement are of paramount importance, which were carried out here using complementary techniques such as optical absorption spectroscopy, X-ray reflectivity, and atomic force microscopy and by tuning the pre-deposition parameters such as solvent, polymer concentration (c), and spinning speed (ω) of the spin-coated D−A copolymer thin films. The high c-value films show unusual improvement of EB with increasing ω, unlike low c-value films, for the first time. The overlapped and entangled aggregates, which are known to form in the high c-value solution of high viscosity, get disentangled in the film during deposition due to a large centrifugal force arising from their relatively large effective mass along with the increasing ω-value. On the contrary, the well separated less entangled aggregates, which formed in the low c-value solution of low viscosity, get entangled in the film due to the ω-related fast evaporation of the solution. Ultimately, improved EB is observed when both c and ω are either small or large for the films prepared using chlorobenzene (CB) and only large for the films prepared using chloroform (CF), which can be realized considering effective evaporation rate and viscosity of the solutions during deposition, while improved EO ordering is found when both c and ω are small (i.e., when diffusion and organization of aggregates are easy) for the films prepared using both the solvents. Altogether, the films prepared using CF with high c and ω values show crystallites with high EB but low EO ordering, while those with low c and ω values show better EO ordering but low EB. The films prepared using CB with low c and ω values show improvement of both EB and EO ordering and thus expected to provide better device performances compared to others.

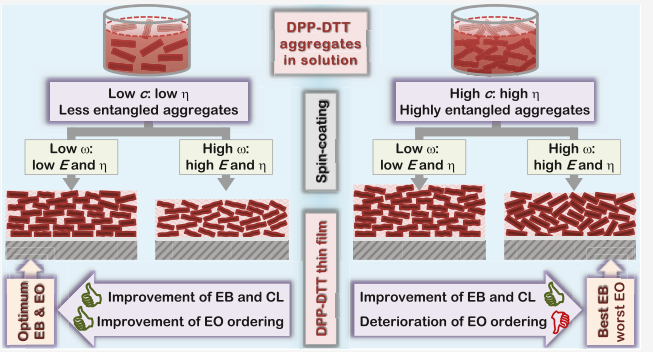

1. INTRODUCTION

Organic molecules and π−conjugated semiconducting polymers having intriguing electrical and optical properties are expected to replace the traditional silicon-based semiconductors partly due to their low cost and large scale fabrication as active layers in opto-electronic devices like organic field effect transistors (OFETs) and organic photovoltaics.[1−6] However, the major problem in commercializing polymeric semiconductor-based OFETs is their low charge carrier mobilities associated with the semicrystalline morphology, arising from the weak intermolecular van der Waals interactions within polymeric molecules.[7] The improvement of the charge carrier mobility of such semicrystalline polymers in general depends on the amount, quality, and orientation of the crystalline aggregates.[8,9] For example, the edge-on orientated (EO) aggregates (where the π−π stacking are parallel to the substrate)[10] are more effective than the face-on orientated aggregates (where the π−π stacking are normal to the substrate),[11] as the EO aggregates allow the charge carriers to flow not only along the conjugated backbone direction but also along the interchain π−π stacking direction.[8] Hence, the improvement of such EO crystallinity, both in terms of quality and quantity, is likely to enhance the charge carrier mobility in the OFET devices.[12,13]

Recently, donor−acceptor (D−A) type copolymers, whose backbone comprises electron-rich and electron-deficient units, in an alternating arrangement, are preferred over homopolymers (consisting of either electron donating or accepting units) as active layers due to their strong intermolecular interaction.[14−18] Such interaction shorten the distance

Received: May 7, 2023
Revised: August 8, 2023
Published: August 22, 2023

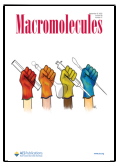

https://doi.org/10.1021/acs.macromol.3c00885
Macromolecules 2023, 56, 7065−7077

between polymer chains (i.e., $\pi-\pi$ stacking separation) and helps in the formation of aggregates, even in solution, both of which play vital roles in efficient charge transport.[19−21] Also, the hybridization of the molecular orbitals between the donor and acceptor units in D−A copolymers typically leads to small band gaps. Altogether, such modification of the π−conjugated cores of a polymeric semiconductor can easily improvise its opto-electronic properties.[22−26] D−A copolymers having diketopyrrolopyrrole (DPP) as an electron-accepting unit and thienothiophene as an electron-donating unit (structural schematic of which is shown in Figure S1 of the Supporting Information) are a subject of extensive research for this purpose due to their easy solution processing.[18,20] The long-branched alkyl side chains, such as octyldodecyl (OD), are usually added to the D−A backbone to make these copolymers soluble in common organic solvents.

Among different solution processing techniques, spin-coating is widely utilized to form polymer thin films, because it can provide smooth uniform films and facilitate large-scale fabrication in less time.[27,28] The structure of a spin-coated thin film heavily depends on three parameters: nature of the solvent, polymer concentration in the solution (c), and spinning speed (ω), apart from the nature of the substrate surface. These parameters determine the film thickness, crystalline quality and ordering, and interfacial (film-substrate and film-air) morphology and/or roughness, all of which play significant roles in tuning charge carrier mobility in OFET. A massive amount of research is going on to understand and tune the structures of D−A copolymer thin films for obtaining better charge carrier mobility.[18,20,29,30] The variation of viscosity of the polymer solution with c was found to show two-regime behavior, with more isolated and extended aggregates at low c and overlapped and entangled aggregates at high c.[31,32] Such nature of aggregates was also found to maintain in the film. However, the effect of ω or solvent on the nature of aggregates of the D−A copolymer thin films is not clear. Understanding of which is very much essential for better charge transport. Further, in an OFET, charge transport takes place either near film-substrate or near film-air interface depending on the contact (bottom-contact or top-contact) of the gate electrode. Thus, it is necessary to have better EO crystallites, both in terms of quantity and quality, in the film, especially near the interfaces, for obtaining improved charge carrier mobility,[33] which can be well understood using X-ray reflectivity (XR) technique.[34−37] The XR technique essentially provides the electron density profile (EDP), i.e., in-plane ($x-y$) average electron density (ρ) as a function of depth (z) in high resolution.[38−40] From the EDP, it is possible to estimate the film thickness, the presence of layering in the film, if any, the surface and interfacial roughness, the structural arrangement near the film-substrate interface and their evolution.[41−44] In fact, the combination of the XR data and the proper modeling scheme, is the state-of-the-art technique for obtaining unique and valuable information about the EO crystallites in the film, especially near the buried interface. On the other hand, optical (UV−vis) absorption spectroscopy can estimate the exciton bandwidth (EB), which can provide the information about the average conjugation length (CL) and/or backbone planarity (BP) of the aggregates.[40,45−48]

In this work, we have utilized the high brilliance synchrotron XR technique to understand the effect of pre-deposition conditions on the out-of-plane structures and EO ordering of spin-coated D−A copolymer thin films, with an emphasis on the EO crystallites near the film-substrate interface, as the improvement of such EO crystallites near the film-substrate interface is very much essential for getting better charge transport for bottom gated OFETs. Basically, the high brilliance synchrotron source can provide relatively wide dynamic range of XR data with better resolution, which helps to remove uncertainties at the time of data analysis.[40] Further, complementary optical absorption technique has been used to obtain the information about the quality of the crystalline aggregates in the film[40,48] and the atomic force microscopy technique to probe the topography of the film.[40,44] Indeed, the orientation and quality of crystalline aggregates are heavily influenced by the choice of solvent (chloroform or chlorobenzene), c, and ω values. The high c-value films show improvement in EB with increasing ω, unlike low c-value films, for the first time. This is a clear indication of a large centrifugal force induced disentanglement of the polymer crystallites in the film during deposition, which were otherwise known to overlap and entangle in the solution and also in the film.[31] On the other hand, increasing ω-value seems to hamper the EO ordering and crystalline quality of the films prepared from low c-value solution, whereas, increasing ω-value seems to improve the EO ordering and crystalline quality of the films prepared from high c-value solution, irrespective of the choice of solvent. Similarly, for fixed ω-value, increasing c-value of the solution seems to deteriorate the EO ordering. An attempt has been made to correlate the observed structures and their variation with the growth parameters. Also, the possible implications of such structures in the device properties are discussed.

2. EXPERIMENTAL SECTION

Poly[2,5-(2-OD)-3,6-diketopyrrolopyrrole-alt-5,5-(2,5-di(thien-2-yl)-thieno[3,2-b]thiophene)] (DPP−DTT) copolymer $[(C_{60}H_{90}N_2O_2S_4)_n$, of average molecular weight 40,000−60,000] was purchased (from Sigma-Aldrich) and used as received. Chlorobenzene (CB, from Sigma-Aldrich) and chloroform (CF, from Merck) were used as solvents to prepare the polymer solutions. Polymer solutions were prepared by dissolving the various amounts of DPP−DTT in CB and CF solvents. Three different concentrations [c = 1.7, 3.5 and 5.0 g L^{-1}] of the polymer in CB solutions and three concentrations [c = 0.8, 1.7 and 3.5 g L^{-1}] of the polymer in CF solutions were prepared. All the solutions were sonicated for 15 min. Sonication for 15 min was found sufficient for the dissolution of the polymer in CF (which acts as a very good solvent) but not in CB. The solutions containing CB were further heated at 60 °C for 5 min for complete dissolution. Before deposition, the Si and quartz glass (QG) substrates (of size about 12 × 12 mm^2) were sonicated in acetone and ethanol to remove the organic contaminates. DPP−DTT films were then deposited on Si and QG substrates using a spin-coater (SCS 6800)[40] at various spinning speeds (ω) for 60 s. The films prepared for c = 1.7 and 5.0 g L^{-1} using CB on Si and QG substrates for different ω-values are labelled as L-CB, L-CB_g (L denotes low c-value) and H-CB, H-CB_g (H denotes high c-value), respectively. Similarly, the films prepared for c = 0.8 and 3.5 g L^{-1} using CF on Si and QG substrates are labelled as L-CF, L-CF_g and H-CF, H-CF_g, respectively. After deposition, all films were subsequently heated at 70−80 °C for 30 min under vacuum condition to remove the residual solvent, if any.

XR measurements of the films were carried out using a synchrotron source (MCX beamline, Elettra)[40,49,50] at an energy 10 keV (i.e., wavelength, λ = 1.24 Å). The beamline was equipped with a diffractometer, which has a four-circle goniometer and a flat sample stage. The latter has two circular and three translational (X, Y, and Z) motions. A Kapton window-based cell was placed on the flat sample stage. The scattered beam was detected using a scintillation detector behind a set of receiving slits. In XR technique, data were taken under specular condition, i.e., the reflected angle is equal to the incident

https://doi.org/10.1021/acs.macromol.3c00885
Macromolecules 2023, 56, 7065−7077

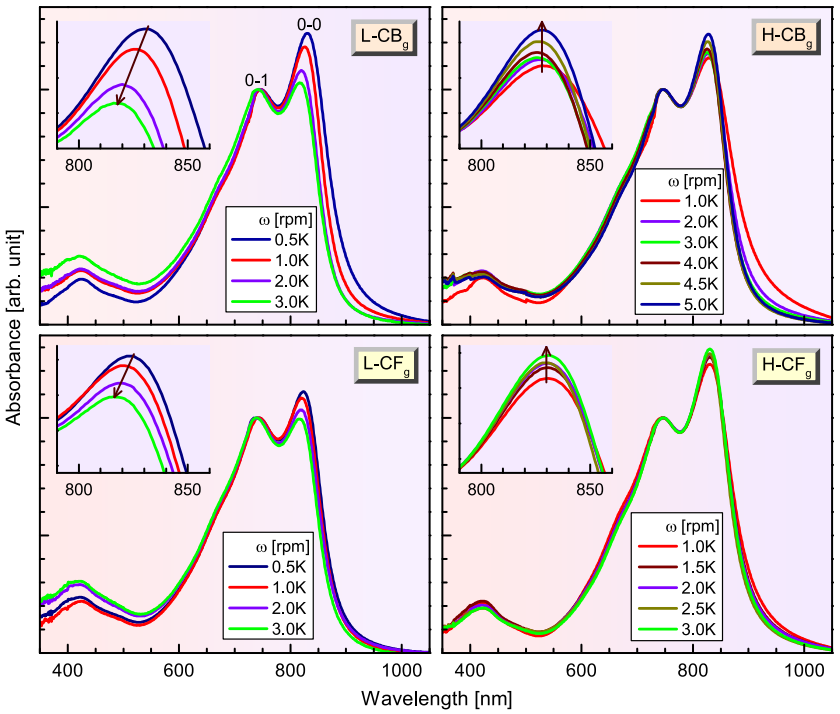

Figure 1. UV−vis absorption spectra (normalized by the 0−1 transition peak intensity) of the DPP−DTT thin films deposited at different spinning speeds (ω) from solutions containing low and high concentrations of the polymer in CB and CF solvents. Insets: magnified view of the selected portion of the spectra to show the evolution of the 0−0 transition peak.

angle, θ. Under such condition, there exists a nonvanishing wave vector component, q_z, which is given by $(4\pi/\lambda)$ sin θ with resolution 0.001 Å $^{-1}$. The XR measurements of all the films were carried out in vacuum, after placing them inside the Kapton window-based cell.

Optical absorption spectra of the DPP−DTT thin films on QGs were recorded using a UV−vis spectrophotometer (JASCO, V-630)[40,48] and the topography of the films were mapped by an atomic force microscope (CSI Nano-Observer).[6,40] Topographic images were collected using Au-coated Si tip (radius of curvature ∼10 nm) in a tapping mode (resonance frequency ∼60 kHz) to minimize tip-induced damage of the soft film. Scans of different sizes and in different portions of the sample were carried out to get statistically meaningful information about the topography. Processing and analysis of the AFM images were carried out using WSXM software.

3. RESULTS AND DISCUSSION

3.1. Optical Absorption and Crystalline Aggregates.

The optical absorption spectra (normalized with the peak intensity near 745 nm) of the DPP−DTT thin films deposited from solutions of two different c-values (low and high) in two different solvents (CB and CF) at different ω-values are shown in Figure 1. Such spectra of the films can be classified into two parts- the lower wavelength part, which reflects the transitions between intrachain states (π−π^* transition around 425 nm) arising from the disordered (coil-like) polymer chains[51] and the higher wavelength part, where the prominent peaks are the transitions between states arising from the aggregated or crystalline (rod-like) polymer chains.[20,52] The aggregated part constitutes of two prominent 0−0 and 0−1 transitions and slightly less intense 0−2 transition, reflecting the presence of strong vibronic fine structures between the ground state (S_0, also known as highest occupied molecular orbital or HOMO) and the first excited state (S_1, also known as lowest unoccupied molecular orbital or LUMO). The presence of distinct vibronic features, in the solution itself (shown in Figure S2 of the Supporting Information), clearly suggests that the polymer chains form crystalline aggregates, even in solution,[53] reflect large coplanarity of the backbones and their strong D−A interactions.

The absorption ratio of the 0−0 and 0−1 vibronic peaks (A_{0-0}/A_{0-1}) is an important parameter to define the photophysical properties or the type of interaction between the polymer chains.[47,48] Here, 0−0 transition dominates over 0−1 transition (i.e., $A_{0-0}/A_{0-1} > 1$), hence its photophysical properties can be best described by the J-aggregate model, where Coulomb coupling is negative.[45,46,54,55] The polymer chains with repeated donor and acceptor units essentially create a negative excitonic coupling between the adjacent monomer units originating from electron and hole transfer along the polymer chain, that results in the formation of more extended conformation or larger CL along the polymer chain, which is very much effective for getting better charge carrier mobilities in the devices. The degree of such intrachain ordering along the polymer backbones or the CL is related to the intrachain coupling strength (J_0) or the free EB ($W = 4|J_0|$) between the repeated monomer units.[47,55] For a J-aggregate system (where $J_0 < 0$), W can be expressed (assuming the Huang−Rhys factor to be unity) as follows:[47]

$$W \approx E_p \frac{\sqrt{A_{0-0}/A_{0-1}} - 1}{0.24 + 0.073\sqrt{A_{0-0}/A_{0-1}}} \quad (1)$$

where E_p is the main intramolecular vibrational energy of the C=C symmetric stretching (assumed to be 0.17 eV).[48] An increase in the A_{0-0}/A_{0-1}-value corresponds to an increase in the W-value and, therefore, an increase in the BP and/or CL. A large A_{0-0}/A_{0-1}-value (∼1.4) for the polymer in solutions indicates a high W-value (∼90 meV) and a remarkable intrachain ordering of the aggregates in both the solvents. A

https://doi.org/10.1021/acs.macromol.3c00885
Macromolecules 2023, 56, 7065−7077

slight red-shift (about 10 nm) of the 0−0 vibronic transition for the polymer in CB solvent indicates more ordered molecular organization (strong $\pi-\pi$ interactions) of the polymer chains within the aggregates in CB as compared to CF, most probably due to less polymer−solvent interaction in case of CB as compared to CF.

To understand the effects of ω, c, and solvent on the crystalline quality or CL of the aggregates in the solid films, the parameters such as the position of the 0−0 transition (λ_{0-0}), A_{0-0}/A_{0-1}, and W for the polymer thin films are listed in Table S1 of the Supporting Information. The variation of W and the energy of the 0−0 transition (E_{0-0}) with ω for the DPP−DTT thin films deposited from solutions of two different c-values (low and high) in two different solvents (CB and CF) are plotted in Figure 2. It is evident from Figure 2 that the

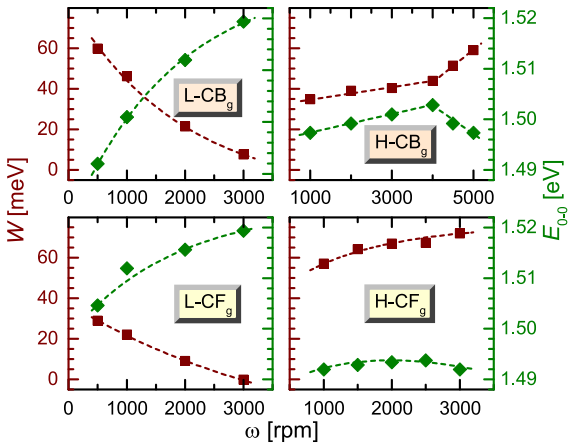

Figure 2. Variation of the free EB (W) and the energy of the 0−0 vibronic transition (E_{0-0}) with spinning speed (ω) for the DPP−DTT thin films deposited from solutions containing low and high concentrations of the polymer in CB and CF solvents.

variation of W for the low c-value films is completely different from that of the high c-value films. It can be noted that the numerical value of W differs depending upon the analysis scheme, however, the trend in the variation of W, which is the main aspect, remains unchanged (as shown in Figures S3 and S4 of the Supporting Information). In case of L-CB$_g$ films, the W-value is quite large for the low ω-value film, which decreases rapidly with the increase of ω-value, while for H-CB$_g$ films, the value is relatively small for the low ω-value film, which increases (initially slow and then fast) with the increase of ω-value. On the other hand, in case of L-CF$_g$ films, a quite small W-value for the low ω-value film decreases further with the increase of ω-value, while for H-CF$_g$ films, the relatively high W-value for the low ω-value film increases further with the increase of ω-value. E_{0-0} is another important parameter, which is related to the HOMO−LUMO gap (plus the exciton binding energy).[48] The variation of E_{0-0} with ω for the low c-value films is totally different from that of the high c-value films. The E_{0-0}-value gradually increases (or blue-shifted) with ω for L-CB$_g$ and L-CF$_g$ films, whereas for H-CB$_g$ and H-CF$_g$ films, the E_{0-0}-value first increases then decreases with ω, though the variation is almost negligible.

In low c-value solution, there is a possibility to getting better intrachain ordering of the polymer chains within the aggregates. As the concentration of the polymer is increased, the intrachain ordering within the aggregates is perturbed due to more chain overlap and chain interpenetration that subsequently reduces the BP within the aggregates.[56] The large W-value for the L-CB$_g$ film with low ω-value suggests a relatively better intrachain ordering of the aggregates in the film. The slow evaporation rate of CB as well as lower spinning speed seem to allow the polymer chains to have more time to relax into more thermodynamically favorable conformation to lead relatively better intrachain ordering of the aggregates (but less than that in solution). The evaporation rate increases with the increase of ω-value, which increases the effective concentration of the polymer solution and the interpenetration of the polymer chains, while restricts the relaxation of the polymer chains to a more extended conformation.[56,57] This subsequently decreases the intrachain ordering of the backbones in the L-CB$_g$ films. It also reduces the $\pi-\pi$ stacking interactions (blue-shift of W) between the polymer chains within the aggregates. In case of L-CF$_g$ film with lower ω-value, a moderate intrachain ordering is observed. Basically, the high evaporation rate of CF reduces the intrachain ordering predominantly during depositions due to rapid increase in the effective concentration of the polymer, even at lower ω-value. The decrease in the intrachain ordering and their subsequent $\pi-\pi$ stacking interactions are also observed for L-CF$_g$ films with further increase in the ω-value, similar to those of the L-CB$_g$ films. On the other hand, the planarity of the backbones within the aggregates in high c-value solution is expected to perturb due to the large entanglement of the polymer chains. On contrary, the $\pi-\pi$ stacking and the CL of the H-CF$_g$ film with low ω-value are found more (from low E_{0-0}-value and high W-value) compared to the L-CF$_g$ film with low ω-value. Also, the intrachain ordering of the backbones is systematically increased with the increase in the ω-value for H-CB$_g$ and H-CF$_g$ films, which is quite surprising. Centrifuge force seems to play important role in extending the planarity of the aggregates when spin-coated from high concentration polymer solutions.[57] Overall, the film with low c- and ω-values shows the best $\pi-\pi$ stacking (as E_{0-0}-value is lowest) and CL (as W-value is highest) among the films deposited from CB, while the film with high c- and ω values shows the best $\pi-\pi$ stacking (lowest E_{0-0}-value) and CL (highest W-value) among the films deposited from CF.

3.2. EDP and EO Crystalline Aggregates. *3.2.1. Effect of Spinning Speed.* XR profiles of the spin-coated DPP−DTT thin films deposited at different spinning speeds from different concentrations of the polymer in CB and CF solvents are shown in Figure 3. The presence of Kiessig fringes,[58] indicative of a total film thickness ($D_K = 2\pi/\Delta q_K$, where Δq_K is the difference between two consecutive Kiessig fringes), is very clearly evident in almost all XR profiles, except for the film deposited from high c-value solution in CF and at low ω-value (1000 rpm), which clearly suggests that the top surface of that particular film is quite rough as compared to the other films. The decrease in Δq_K value, hence the increase in film thickness (D_K), with the increase of the polymer concentration and with the decrease in the spinning speed are observed for both solvents, as expected. Apart from speed and concentration, the Kiessig fringes were also found to depend on the nature of solvent. For the films deposited with same c and ω values, the thickness of the film prepared with CF solvent is higher as compared to the film prepared with CB solvent. Sharp peaks near $q_z \approx 0.31$ and 0.62 Å^{-1} are evident in almost all the XR profiles, which corresponds to the 1st and 2nd order Bragg peaks of the EO ordered layers of DPP−DTT. The positions

https://doi.org/10.1021/acs.macromol.3c00885
Macromolecules 2023, 56, 7065−7077

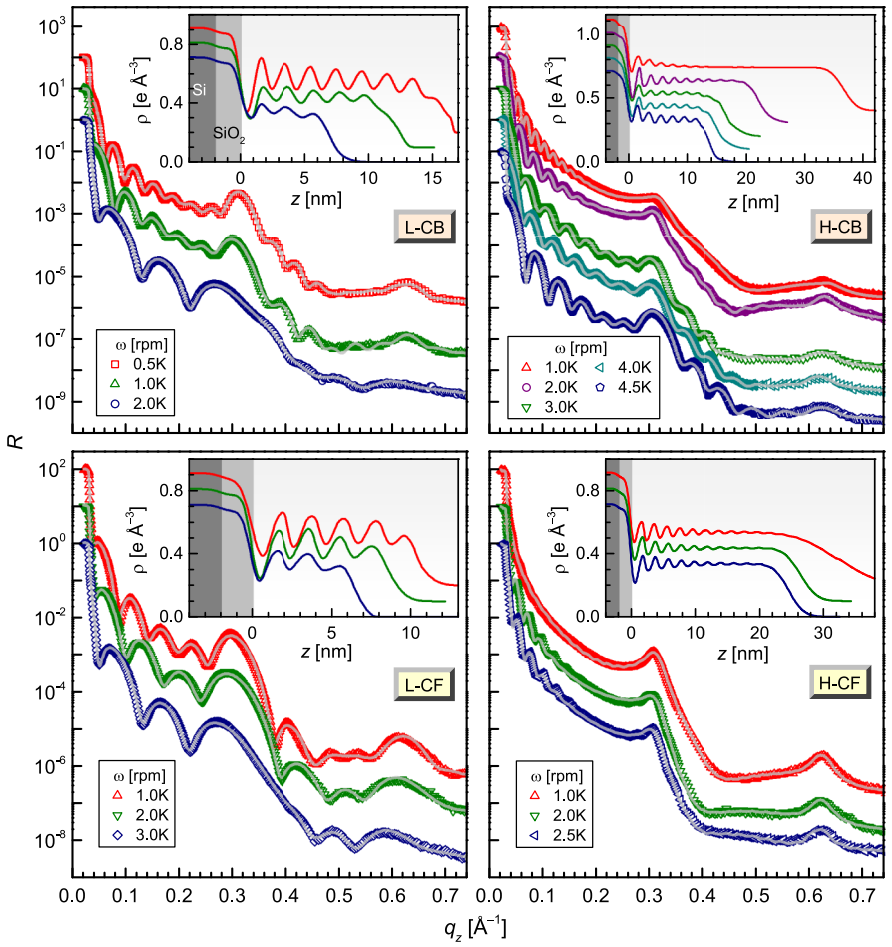

Figure 3. Evolution of XR profiles (symbols) and analyzed curves (solid lines) with spinning speed (ω) for the DPP−DTT thin films deposited from the solutions containing low and high concentrations of the polymer in CB and CF solvents. Insets: corresponding analyzed EDPs. Curves and profiles are shifted vertically for clarity.

of such peaks provide the lamellar thickness (d), while the width of such peaks provide the crystallite size of the EO ordered aggregates along the out-of-plane direction of the film. From XR profiles, it is clear that the intensity and widths of such Bragg peaks are significantly varied with c and ω-values. This means that the ordering of such EO crystallites strongly depends on the pre-deposition conditions.

To get proper information about the effects of pre-deposition conditions on the EO ordering of the aggregates in the film, especially near the film-substrate interface, the XR data were analyzed quantitatively using matrix method after incorporating roughness at each interface.[36,37] An instrumental resolution in the form of a Gaussian function and a constant background were also included at the time of data analysis.[40] The models with gradual evolution, relevant for the XR data analysis, are shown schematically in Figure 4 to understand the analysis and to correlate the parameters with the film structures. For the analysis, each film of thickness, D, was divided into a number of lamellar, after incorporating an interfacial oxide layer above the substrate.[48,59] Each lamellar represents a bilayer of thickness d consists of a high electron density (ρ_{bb}) fused-aromatic backbone layer of donor and acceptor moieties of thickness d_{bb} and a low electron density (ρ_{sc}) alkyl-side chain layer of thickness d_{sc} (as shown schematically in Figure 4). The uniform electron density contrast between the backbone and alkyl-side chain layers (i.e., $\Delta\rho = \rho_{bb} - \rho_{sc}$) along the z-direction of the film was unable to fit the XR data properly at the time of data analysis. In order to overcome this problem, further variation of $\Delta\rho$ along the z-direction was considered.[40,48] As the slow evaporation of the solvent near the film−substrate interface (i.e., larger time) is likely to help the organization of the crystalline aggregates and their ordering near that interface, while the fast evaporation of the solvent near the film−air interface (i.e., lesser time) is likely to restrict the organization of the crystalline aggregates and their ordering at the top; the variation of $\Delta\rho$ as a function of film thickness was expressed as follows:

$$\Delta\rho(nd) = \Delta\rho_m \exp(-nd/\zeta) \quad (2)$$

where n is an integer, $\Delta\rho_m$ is the maximum electron density contrast, and ζ is the critical decay length. The large value of $\Delta\rho_m$ is related to the better in-plane EO ordering of the crystalline aggregates near the film−substrate interface, which is particularly important to get better mobilities of the film and a large value of ζ indicates a better extent of EO ordering along out-of-plane direction, which is related to the improvement of the in-plane EO ordering of the aggregates near the film-air interface. From eq 2, the variations of ρ_{bb} (peak) and ρ_{sc} (dip) with the film thickness can be written as follows:

$$\rho_{bb}(n'd) = \rho_a + (d_{sc}/d)\Delta\rho_a \exp(-n'd/\zeta) \quad (3)$$

https://doi.org/10.1021/acs.macromol.3c00885
Macromolecules 2023, 56, 7065−7077

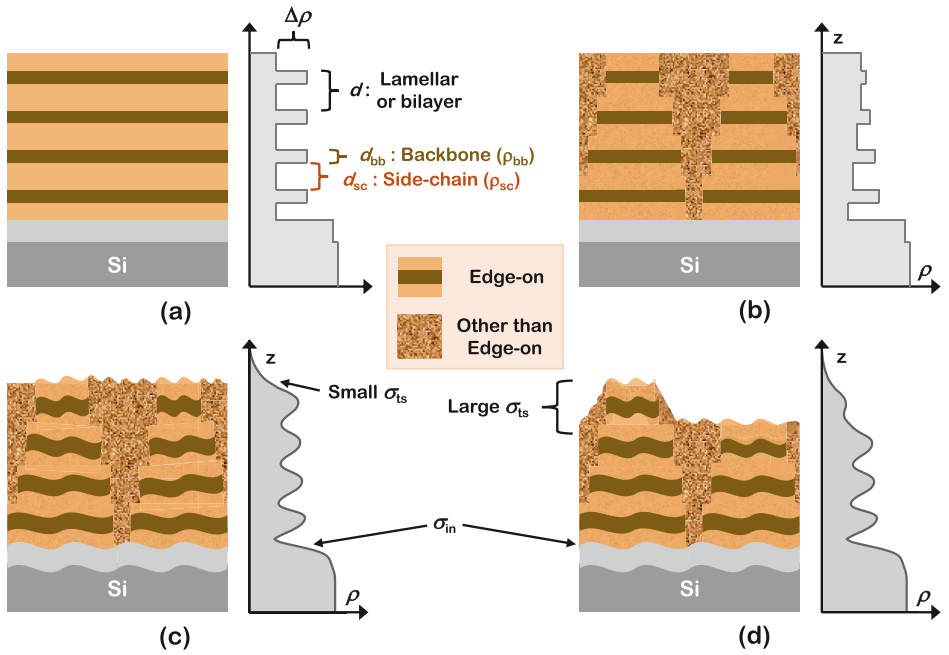

Figure 4. Structural schematics and EDPs corresponding to the different models relevant for the XR data analysis of the film. (a) Perfect edge-on ordering with no roughness at any interface. (b) Decreasing edge-on ordering along z-direction with no roughness at any interface. (c) Decreasing edge-on ordering along z-direction with roughness at each interface (corresponding to the orientation of the crystallites). (d) Decreasing edge-on ordering along z-direction with roughness at each interface and large surface roughness (corresponding to the large variation in the thickness in the film). Different parameters relevant for the analysis are indicated.

$$\rho_{sc}(nd) = \rho_a - (d_{bb}/d)\Delta\rho_a \exp(-nd/\zeta) \quad (4)$$

where, $n' = n + 1/2$ and ρ_a is the average electron density of the film. Here, the terms d_{sc}/d and d_{bb}/d (where $d_{sc}/d_{bb} > 1$) are used because the deviation of ρ_{bb} is more as compared to ρ_{sc} w.r.t. the average electron density ρ_a. At the time of data analysis, a separate interfacial bilayer was also included to take care of effect of substrate boundary conditions including surface energy, if any, on the growth of the film. Basically, here eqs 2−4 are used for the second bilayer onward, i.e., $n = 0$ and $\Delta\rho_m$ represent the position and the maximum electron density contrast, respectively of the second bilayer.

The best-fit XR profiles and the corresponding EDPs thus obtained for the DPP−DTT thin films are presented in Figure 3. Also, the variation of $\Delta\rho$ as a function of z and nd are plotted in Figure 5 to understand the effect of ω on the EO ordering of the aggregates. The relevant parameters, such as D, d, the interfacial roughness (σ_{in}), the top surface roughness (σ_{ts}), $\Delta\rho_m$, and ζ for the DPP−DTT films as obtained from the analyzed EDPs, are listed in Table S2 of the Supporting Information. A low-density layer or dip near the film-substrate interface is observed in the EDP, which clearly indicates that the attachment of the film (i.e., mainly the EO aggregates) with the substrate is through alkyl side chains. A small value of σ_{in} is evident for the films, which indicates a smooth attachment of those alkyl side chains with the substrate, while a high value of σ_{ts} mainly for H-CB and H-CF films is observed, which is probably due to the variation in the number of layers in the film and/or presence of randomly oriented aggregates toward top surface. The value of d obtained here is consistent with that reported before.[25,26] A slight decrease in the d-value with the decrease of ω is observed, which is probably due to the slight interdigitization of the polymer side chains in the films of higher thickness as compared to the film of lower thickness.

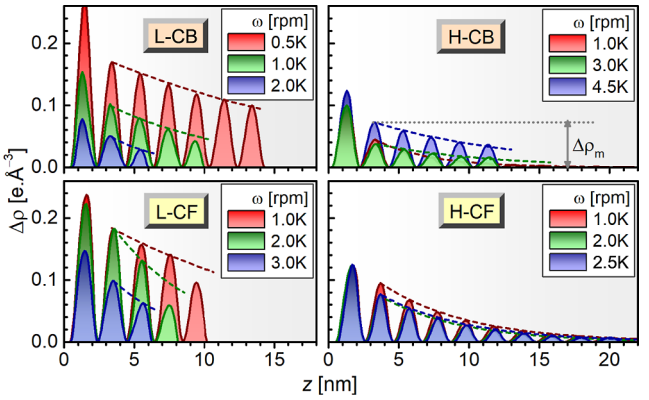

Figure 5. Variation of electron density contrast ($\Delta\rho$) as a function of height (z) for the DPP−DTT thin films deposited from solutions of two different concentrations of the polymer (low and high) in two different solvents (CB and CF) at different spinning speeds (ω).

To understand the evolution of EO structure in the films with spinning speed for different concentrations, the variations of D, ζ, and $\Delta\rho_m$ with ω are plotted in Figure 6. The D-value and its gradual decrease with increasing ω are found to depend on c and solvent, as expected. A reasonable EO ordering is evident for the films having thickness less than about 20 nm and not much EO ordering beyond that thickness. This suggests that the EO ordering of the aggregates predominantly takes place near the substrate and extends up to few layers. The variation of $\Delta\rho_m$ with ω for the L-CB and L-CF films are found quite high compared to the H-CB and H-CF films. This suggests that the effect of spinning speeds on the EO crystallites near the film−substrate interface is more for the films prepared with low c-value solution as compared to the film prepared with high c-value solution. A larger $\Delta\rho_m$-value is observed for the films prepared with lower ω-value among the

https://doi.org/10.1021/acs.macromol.3c00885
Macromolecules 2023, 56, 7065−7077

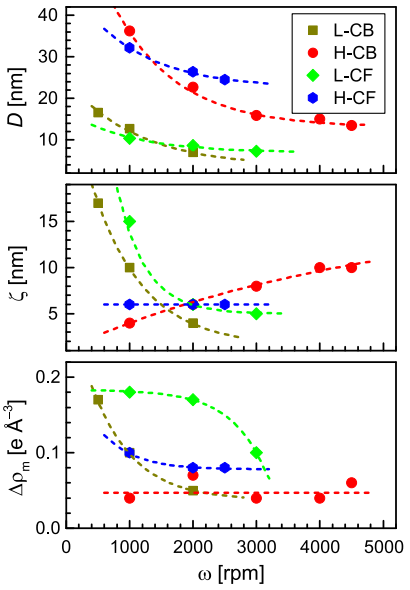

Figure 6. Variation of film thickness (D), decay length (ζ), and maximum electron density contrast ($\Delta\rho_m$) with spinning speed (ω) for the DPP−DTT thin films deposited from solutions of two different polymer concentrations (low and high) in two different solvents (CB and CF).

L-CB and L-CF films. As the value of ω is increased, the $\Delta\rho_m$-value is decreased systematically. For L-CB films, the decrease in $\Delta\rho_m$-value is more at higher ω-value, whereas, a still large value of $\Delta\rho_m$ is seen at higher ω value for L-CF films. For H-CF films, a similar effect of ω on $\Delta\rho_m$-value is observed, but in case of H-CB films, the variation of $\Delta\rho_m$ with ω is not systematic. The variation of ζ with ω is found really interesting. For the low c-value films, ζ decreases gradually with the increase of ω, while for the high c-value films, ζ either remains same or increases gradually with the increase of ω. Overall, $\Delta\rho_m$ and ζ parameters are found high for the films with low c and ω values. That means that the low spinning speed provides enough time for the low concentration solution, to organize the crystallites in preferred EO ordering, not only near the film−substrate interface but also throughout the film.

3.2.2. Effect of Solvent. The EO ordering of the aggregates also depends on the nature of the solvent, as evident from the XR data and the analyzed EDPs of the DPP−DTT thin films (in Figure S5 of the Supporting Information). The EO ordering of the aggregates near the film−substrate interface is found slightly better (from $\Delta\rho_m$-value) for the film deposited with CF as compared to the film deposited with CB. Whereas, a slightly better EO ordering of the aggregates near the film−air interface is observed (from ζ-value) for the film deposited with CB as compared to the film deposited with CF. Basically, the viscosity of the solvent (η_0) effectively controls the organization and ordering of such aggregates near the film−substrate interface, whereas the organization and ordering of the aggregates toward the film−air interface mainly depends on the solvent evaporation rate (E).[60] The low η_0-value of CF (0.54 cP) as compared to CB (0.75 cP) is likely to help the diffusion of the aggregates to promote a slightly better in-plane EO ordering of the aggregates near the film-substrate interface. On the other hand, the low E-value of CB (1.1) as compared to CF (11.1) provides more time for the organization of the aggregates toward the film-air interface that leads to an increase in the extent of EO ordering of the aggregates along out-of-plane direction of the film.

3.2.3. Effect of Concentration. The XR profiles and the EDPs of the DPP−DTT thin films deposited from solutions of different c-values are plotted separately (in Figure S6 of the Supporting Information) to see the effect of concentration. It is evident from the EDPs that the concentration, apart from ω and solvent, plays a significant role on the organization of the EO aggregates in the film, particularly near the film-substrate interface. The variation of $\Delta\rho$ as a function of z for those films are plotted in Figure 7 and the corresponding analyzed parameters are listed separately in Table S2. With the increase in c-value, though there is an insignificant change in the σ_{in}-value, the σ_{ts}-value increases significantly, probably due to the variation in the number of layers in the film and/or an increase in the randomness of the orientation of the aggregates near the top surface of the film. For better understanding the effect of concentration on the organization and ordering of EO crystallites, the variation of D, ζ, and $\Delta\rho_m$ with c are plotted in Figure 8. D increases with c, as expected. A large $\Delta\rho_m$-value is observed for the film deposited with low c-value (1.7 g L^{-1}) solution of CB, which remains almost unchanged for the film deposited with c = 3.5 g L^{-1}, while reduces significantly for the film deposited with high c-value (5 g L^{-1}). Similarly, a larger $\Delta\rho_m$-value is obtained for the film prepared with low c-value (0.8 g L^{-1}) solution of CF, which decreases significantly for the film prepared with c = 1.7 g L^{-1} and further slightly for the film prepared with high c-value (3.5 g L^{-1}). This indicates a better

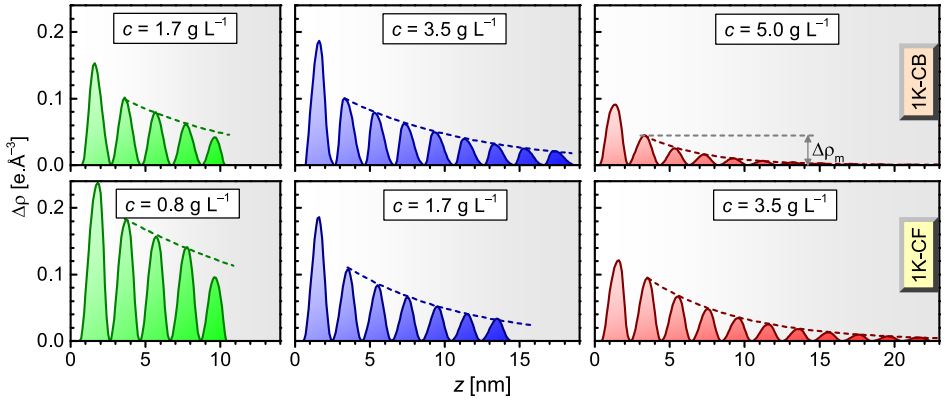

Figure 7. Variation of electron density contrast ($\Delta\rho$) as a function of height (z) for the DPP−DTT thin films deposited from solutions containing different concentrations of the polymer (c) in two different solvents (CB and CF) at a fixed spinning speed (ω = 1000 rpm).

https://doi.org/10.1021/acs.macromol.3c00885
Macromolecules 2023, 56, 7065−7077

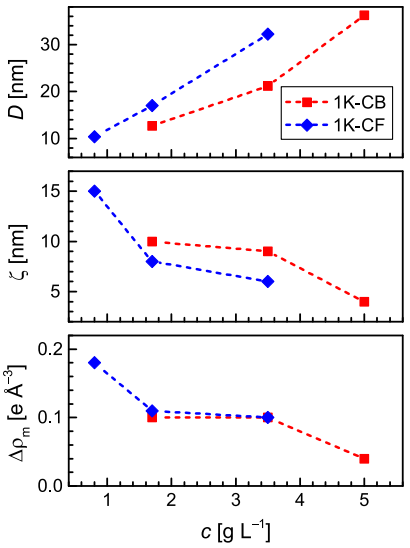

Figure 8. Variation of film thickness (D), decay length (ζ), and maximum electron density contrast ($\Delta\rho_m$) with polymer concentration (c) in two different solvents (CB and CF) for the DPP−DTT thin films deposited at a fixed spinning speed (ω = 1000 rpm).

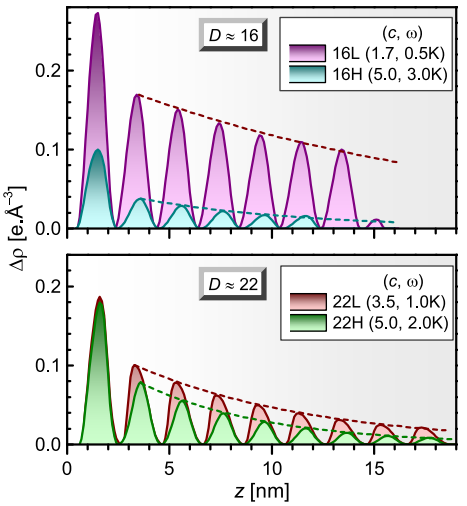

Figure 9. Variation of electron density contrast ($\Delta\rho$) as a function of height (z) and in bilayer steps (nd) for the DPP−DTT thin films of two different sets of film thickness, each set with different combinations of polymer concentration (in the CB solvent) and spinning speed (c, ω).

in-plane EO ordering (larger $\Delta\rho_m$-value) of the crystalline aggregates near the film-substrate interface for the film deposited with lower c-value solutions, whereas lesser in-plane EO ordering of the aggregates near the film−substrate interface (lower $\Delta\rho_m$-value) for the film deposited with higher c-value solutions. Basically, the large c-value increases the effective viscosity (η-value) of the solution[31] that restricts the diffusion and the organization of the aggregates throughout the film (as evident from small $\Delta\rho_m$ and ζ values). On the other hand, small c-value, lowers the η-value and enhances the diffusion of the aggregates to promote the EO ordering of the film near the film-substrate interface (large $\Delta\rho_m$-value) and its extent along the out-of-plane direction (large ζ-value).

3.2.4. Combined Effect of Speed and Concentration. In order to figure out the combined effect of speed and concentration on the organization and ordering of the EO crystallites, the films of nearly same thickness but obtained from two different combinations of c and ω (one with low c and ω values and other with relatively high c and ω values) were considered. Films of two different thicknesses ($D \approx 16$ and 22 nm), obtained from solution containing CB, are discussed here. 16-nm thick film obtained from c = 1.7 g L^{-1} and ω = 500 rpm is labelled as 16L, while that obtained from c = 5 g L^{-1} and ω = 3000 rpm is labelled as 16H. Similarly, 22-nm thick film obtained from c = 3.5 g L^{-1} and ω = 1000 rpm is labelled as 22L, while that obtained from c = 5 g L^{-1} and ω = 2000 rpm is labelled as 22H. The variation of $\Delta\rho$ as a function of z of these films are shown in Figure 9, which are obtained from the XR profiles and their analyzed EDPs (as shown in Figure S7 of the Supporting Information). Corresponding analyzed parameters are listed separately in Table S2. The values of $\Delta\rho_m$ and ζ are found significantly large for the 16L film as compared to the 16H film and those for the 22L film are found slightly large compared to the 22H film. Further, the σ_{in}-value for the 16L film is observed small compared to the 16H film and for the 22L film is found slightly small compared to the 22H film. This result indicates that the combination of low c and ω values makes the attachments of the aggregates with the substrate smooth (small σ_{in}-value) and the EO arrangement of the aggregates more organized or ordered near the film-substrate interface (large $\Delta\rho_m$-value) as well as toward the film−air interface (large ζ-value). Whereas, the combination of high c and ω values seems to make the attachments of the aggregates with substrate slightly rough (high σ_{in}-value) and subsequent EO arrangement of the aggregates less organized or ordered near the film-substrate interface (small $\Delta\rho_m$-value) and also toward the film-air interface (small ζ-value). It is also observed that the decrease of $\Delta\rho_m$ and ζ with z for the 16H film is more compared to that of the 16L film due to large variation of c and ω during deposition, while the decrease of those parameters for the 22H film is quite less as compared to that of the 22L film, most probably due to small variation of c and ω during deposition.

3.3. Topography and Orientation of EO Aggregates.

AFM images of the 16L and 16H films, of similar thickness but different combination of c and ω values, for which the organizations of the EO crystallites throughout the film are substantially different (as evident from values of $\Delta\rho_m$ and ζ), are shown in Figure 10. It is apparent from those topographical images that both the films are composed of similar fiber-like aggregates.[29] The effective in-plane width of those fibers in the 16L film seems to be more compared to the 16H film. To quantify this, the power spectral density (PSD) profiles for the two films, obtained from the AFM images, are shown in Figure 10. It can be noted that the PSD is the angular averaged radial distribution of the Fourier transformed height fluctuation data (AFM image).[59,61] The wave vector (k), where a major change in the slope of PSD profile takes place, corresponds to a certain in-plane correlation length in the system. The correlation length (ξ) that is obtained here from the k-value indicated by the dashed line in the PSD profile (Figure 10) can be correlated with the in-plane width of the fibers. The effective width of the fibers in the 16L film ($\xi \approx 220$ nm) is indeed found more compared to the 16H film ($\xi \approx 180$ nm). This result is consistent with the optical absorption and the XR results, namely the lesser entangled and better EO ordered aggregates in the 16L film are expected to show up as fibers with larger in-plane width, while the greater entangled and

https://doi.org/10.1021/acs.macromol.3c00885
Macromolecules 2023, 56, 7065−7077

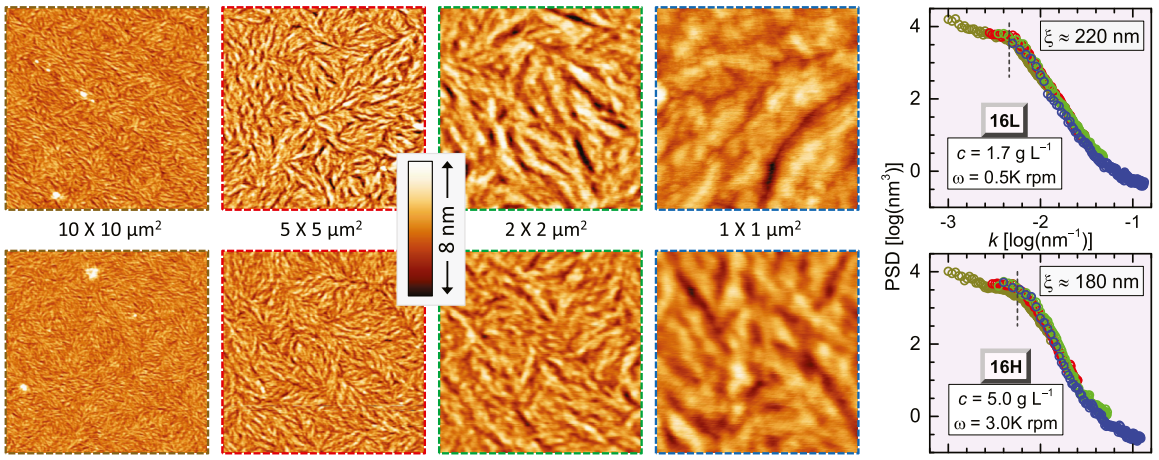

Figure 10. Typical AFM images (in four different scan sizes) and corresponding PSD profiles of two DPP−DTT thin films (16L and 16H) of nearly same thickness ($D \approx 16$ nm) but of different combinations of polymer concentration and spinning speed (c and ω, as indicated). The in-plane correlation lengths (ξ) estimated from the specific positions of the wave vector (k, marked by dashed lines) are indicated.

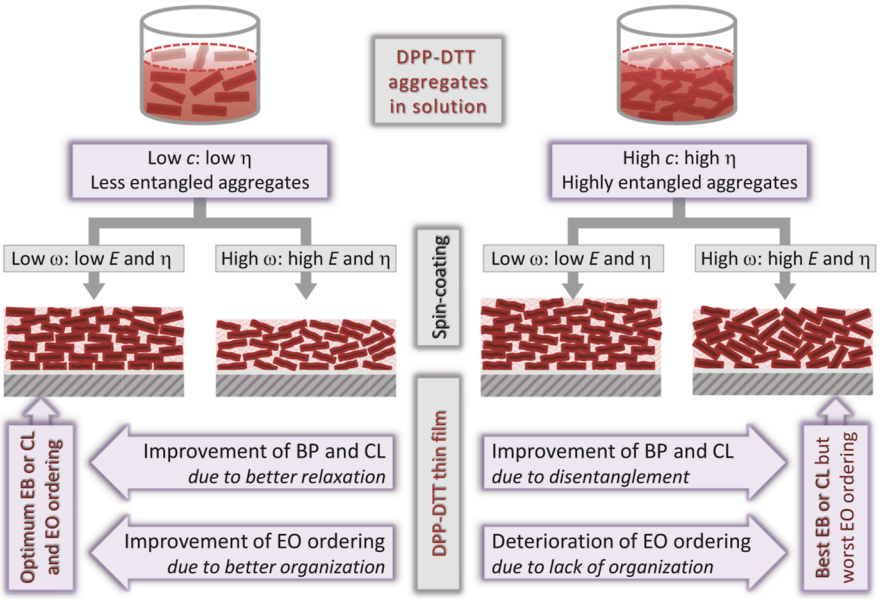

Figure 11. Schematic illustration of the growth and organization of DPP−DTT aggregates. Low c solution, containing well separated less entangled aggregates, formed films with improved BP or CL and EO ordering (through better relaxation and organization) at low ω, while deteriorated BP or CL and EO ordering (through excessive stretch and less organization) at high ω. High c solution, containing highly entangled merged aggregates, formed films with deteriorated BP or CL but reasonable EO ordering (due to entanglement and good organization) at low ω, while remarkably improved BP or CL but deteriorated EO ordering (through proper disentanglement and less organization) at high ω.

relatively poor EO ordered aggregates in the 16H film are likely to show up as fibers with relatively shorter effective in-plane width.

3.4. Overall Structure and Its Implication in Charge Transport. Let us now try to understand the growth, structure, and organization of the aggregates in the DPP−DTT thin films, in terms of the choice of solvent, c, and ω, from the information accumulated from optical absorption, XR, and AFM measurements and also try to comment on the possible effects of different structures on the charge transport. Basically, the repeated electron-accepting (DPP) and electron-donating (DTT) monomer units in the DPP−DTT polymer create large intrachain ordering and planarity along the polymer chains through intramolecular charge transfer from donor to acceptor units. Such a large BP along the polymer chain and strong D−A interactions between the adjacent polymer chains help to promote the $\pi-\pi$ stacking to form aggregates in the solution state. The formation of aggregates with better intrachain order or large CL, even in the solution state, is the possible reason to get better charge carrier mobility of these D−A type copolymers as compared to the conventional homopolymers. However, irrespective of the solvent, the percentage of aggregates somewhat remains almost same, though the quality (ordering) changes slightly.[53] So, tuning aggregate percentage through solvent−polymer interaction is not a good idea, though poor or marginal solvent can induce larger aggregates.[21] Apart from solvent−polymer interaction, E and η values of the solvent play a massive role in determining the thin film structure. Also, the ω and c values strongly influence the E and η values of the solution during spin coating and hence the film structures. Thus, combination

https://doi.org/10.1021/acs.macromol.3c00885
Macromolecules 2023, 56, 7065−7077

of solvent, c and ω ultimately decide the structure of the film as shown schematically in Figure 11.

It can be noted that though grazing incidence wide angle X-ray scattering can provide the overall information about the orientation of the crystalline aggregates, XR is the best technique for obtaining the details of the edge-on ordering (especially its variation along z-direction), which is one of the main themes of this work. The XRD map, obtained from specular and plus off-specular XR scans, around lamellar Bragg peak (shown in Figure S8 of the Supporting Information) provides some information about the orientation of the crystallites. Also, the XR profile itself can provide information about the orientation of the crystallites to some extent through proper modelling of the EDP as the presence of only perfect EO crystallites creates sharp interface within a bilayer, while the additional presence of EO deviated crystallites decreases that sharpness (i.e., increases the interface roughness) and the further presence of randomly oriented crystallites and/or amorphous polymer, decreases the electron density contrast and increases the dip electron density (as shown in Figure 4). The only problem with XR technique is that it cannot differentiate the randomly oriented crystals from the amorphous part. The structural model that has been proposed here (in Figure 11) is based on the information obtained from the XR data analysis and the quality of aggregates obtained from the optical absorption results.

The E-value increases when ω-value is increased, while η-value increases when c-value is increased. For a fixed c- and ω-values, thin films with CF have higher D-values as compared to those with CB due to higher E-value of CF compared to CB. The expected deterioration of BP (decrease of W-value) with increasing ω in low c-value films is due to the increased E induced entanglement during deposition of the well separated less entangled aggregates in solution, while the unexpected improvement of BP (increase of W-value) with increasing ω in high c-value films is due to the increased centrifugal force induced disentanglement during deposition of the large size overlapped and entangled aggregates in solution.[31,62,63] The radial distance average centrifugal force experienced by any aggregate during spin coating is related to its mass apart from the spinning speed.[63] It is well expected that the overlapped and entangled aggregates, which are known to form in the high c-value solution of high viscosity regime, will have effective mass (m^*) much larger than that (m) of the well separated less entangled aggregates formed in the low c-value solution of low viscosity regime.[31,32] Such relatively large effective mass ($m^* \gg m$) along with the increasing ω creates a large centrifugal force on the entangled aggregates during spin coating to disentangle them. Major improvement of BP (increase of W-value) is observed when both c and ω are either small or large for the films prepared using CB and only large for the films prepared using CF, which can be realized considering low E and high η values of CB compared to CF. In addition to the BP, the EO ordering was also influenced by solvent, c, and ω. Independent of the solvent and c, higher ω increases E, which reduces the time for the organization of aggregates to hamper the EO ordering (lower $\Delta\rho_m$-value), while low c- and ω-value reduce the values of η and E, respectively, which enhance the time for organization and/or diffusion of the aggregates to promote EO ordering (large $\Delta\rho_m$-value).[40] Thin films of same D value can be formed by selecting the values of c and ω either high or low. However, the thin films formed with low c- and ω-values show much better EO ordering (large $\Delta\rho_m$-value) compared to the films formed with high c- and ω-values. Ultimately, the thin film formed with low c- and ω-values using CB shows the best structure considering the BP (large W-value obtained from optical absorption) and EO ordering (large $\Delta\rho_m$ and ζ-values obtained from XR) of the crystalline aggregates and their in-plane width (as obtained from AFM) through optimized diffusion, organization, and relaxation during spin-coating.

Optoelectronic properties of the organic or polymer thin films, in general, depend on the CL or BP (or the W-value). Accordingly, DPP−DTT films prepared from CB at low or high c and ω values, having high BP ($W \approx 60$ meV), are expected to show good charge transport properties. Similarly, DPP−DTT films prepared from CF at high c but different ω values, having higher BP ($W \geq 60$ meV) are expected to show better charge transport, while that at high c and ω values, having highest BP ($W \approx 70$ meV) is expected to show best charge transport properties. The hole mobility of DPP−DTT based structure was found to improve with the increase of its packing density.[26] However, in OFETs, where in-plane charge transport is important, EO ordering also plays a major role. Additionally, OFETs can have different configurations depending on the position of the gate, source, and drain electrodes.[64] In case of bottom-gated OFET, charge accumulation layer is formed (i.e., charge transport takes place) near film-substrate interface, whereas, for top-gated OFET, charge transport takes place near film-air interface. Here, irrespective of the pre-deposition parameters, the EO ordering is maximum near the film-substrate interface. Hence, the bottom gate configuration is preferred over the top gate configuration. However, that maximum EO ordering ($\Delta\rho_m$) and its extent along z-direction (ζ) vary significantly with the pre-deposition parameters. Accordingly, the film like 16L (prepared at low c and ω values using CB), having crystallites with excellent BP ($W \approx 60$ meV), EO ordering ($\Delta\rho_m \approx 0.2$ e Å^{-3} and $\zeta \approx 20$ nm), and in-plane width ($\xi \approx 220$ nm), is likely to provide best charge carrier mobility and device properties.

It can be noted that for the top-gated OFET, the EO ordering in the film near the surface can be checked using near edge X-ray absorption fine structure spectroscopy,[21] but not to distinguish between crystalline and amorphous regions.[65] On the other hand, for the bottom-gated OFET, it is even extremely difficult to single out the EO ordering near the film-substrate interface using different available techniques.[55,66] In this perspective, present analysis and final results are quite novel and unique, which could possibly enhance the understanding about the charge transport in OFET devices. Also, for the films prepared using CF with high c and ω values, where crystallites show high EB but low EO ordering, further studies through different treatments are important to check the possibility of the improvement of the EO ordering maintaining the high EB, which could then lead to a remarkable in-plane charge transport and device performances.

In summary, the effect of pre-deposition conditions during spin-coating (mainly solvent, c and ω) on the growth, structure, and orientation of the aggregates in the DPP−DTT thin films, obtained from complementary XR, UV−vis, and AFM techniques, were presented. Fiber-like aggregates on the surface of the films were observed through AFM, whereas the information about the EO ordering of such aggregates in the films and the BP or EB of the copolymer aggregates were obtained using XR and UV−vis techniques, respectively. The films formed with high c-value solution show unexpected

https://doi.org/10.1021/acs.macromol.3c00885
Macromolecules 2023, 56, 7065−7077

improvement of EB or *W*-value with increasing ω due to the increased centrifugal force induced disentanglement during deposition of the large size overlapped and entangled aggregates in solution. On the contrary, the deterioration of EB with increasing ω in low *c*-value film due to the ω-related fast evaporation of the solution that subsequently entangled the well-separated less-entangled aggregates in solution. A significant improvement in BP (increase in *W*-value) is found when both *c* and ω are either small or large for the films prepared using CB and only large for the films prepared using CF. This can be realized considering the low *E* and high η values of CB in comparison to CF. A significant improvement of EO ordering is observed when both *c* and ω are small (i.e., when organization and diffusion of the aggregates are easy). Ultimately, the films prepared using CF with high *c* and ω values show high BP but low EO ordering and those with low *c* and ω values show better EO ordering but low EB, that means the partial improvement, while the film prepared using CB with low *c* and ω values show excellent BP, EO ordering, and in-plane width of the fiber, and thus expected to show better device performances as compared to others.

■ ASSOCIATED CONTENT

Supporting Information

The Supporting Information is available free of charge at https://pubs.acs.org/doi/10.1021/acs.macromol.3c00885.

Structure of DPP−DTT copolymer; optical absorption spectra of DPP−DTT in solutions; parameters obtained from optical absorption spectra and XR profiles; effects of solvent, concentration, and speed-concentration; and information about orientation of crystallites from the XRD map (PDF)

■ AUTHOR INFORMATION

Corresponding Author

Satyajit Hazra − *Saha Institute of Nuclear Physics, A CI of Homi Bhabha National Institute, Kolkata 700064, India;* orcid.org/0000-0001-5592-2078; Email: satyajit.hazra@saha.ac.in

Authors

Saugata Roy − *Saha Institute of Nuclear Physics, A CI of Homi Bhabha National Institute, Kolkata 700064, India*

Md Saifuddin − *Saha Institute of Nuclear Physics, A CI of Homi Bhabha National Institute, Kolkata 700064, India;* orcid.org/0000-0003-1416-3081

Subhankar Mandal − *Saha Institute of Nuclear Physics, A CI of Homi Bhabha National Institute, Kolkata 700064, India;* orcid.org/0000-0001-8730-5920

Jasper R. Plaisier − *Elettra—Sincrotrone Trieste S.C.p.A., Trieste 34149, Italy;* orcid.org/0000-0003-1981-1498

Complete contact information is available at: https://pubs.acs.org/10.1021/acs.macromol.3c00885

Notes

The authors declare no competing financial interest.

■ ACKNOWLEDGMENTS

The financial support received from DST and Elettra under the Indo-Italian PoC to carry out XR experiments at the MCX beamline of Elettra is thankfully acknowledged. M.S. acknowledges University Grant Commission (UGC), India, and S.M. acknowledges Council of Scientific and Industrial Research (CSIR), India, for providing research fellowship.

■ REFERENCES

(1) Burroughes, J. H.; Bradley, D. D. C.; Brown, A. R.; Marks, R. N.; Mackay, K.; Friend, R. H.; Burns, P. L.; Holmes, A. B. Light-Emitting Diodes Based on Conjugated Polymers. *Nature* **1990**, *347*, 539−541.

(2) Liang, Y.; Xu, Z.; Xia, J.; Tsai, S.-T.; Wu, Y.; Li, G.; Ray, C.; Yu, L. For the Bright Future-Bulk Heterojunction Polymer Solar Cells with Power Conversion Efficiency of 7.4%. *Adv. Mater.* **2010**, *22*, E135−E138.

(3) Facchetti, A. π-Conjugated Polymers for Organic Electronics and Photovoltaic Cell Applications. *Chem. Mater.* **2011**, *23*, 733−758.

(4) Wang, T.; Pearson, A. J.; Lidzey, D. G. Correlating Molecular Morphology with Optoelectronic Function in Solar Cells Based on Low Band-gap Copolymer: Fullerene Blends. *J. Mater. Chem. C* **2013**, *1*, 7266−7293.

(5) Reynolds, J. R.; Thompson, B. C.; Skotheim, T. A. *Conjugated Polymers: Properties, Processing, and Applications*; CRC Press, 2019.

(6) Mandal, S.; Mukherjee, M.; Hazra, S. Evolution of Electronic Structures of Polar Phthalocyanine−Substrate Interfaces. *ACS Appl. Mater. Interfaces* **2020**, *12*, 45564−45573.

(7) Dimitrakopoulos, C. D.; Malenfant, P. R. Organic Thin Film Transistors for Large Area Electronics. *Adv. Mater.* **2002**, *14*, 99−117.

(8) Sirringhaus, H.; Brown, P. J.; Friend, R. H.; Nielsen, M. M.; Bechgaard, K.; Langeveld-Voss, B. M. W.; Spiering, A. J. H.; Janssen, R. A. J.; Meijer, E. W.; Herwig, P.; de Leeuw, D. M. Two-Dimensional Charge Transport in Self-Organized, High-Mobility Conjugated Polymers. *Nature* **1999**, *401*, 685−688.

(9) Kline, R. J.; McGehee, M. D.; Toney, M. F. Highly Oriented Crystals at the Buried Interface in Polythiophene Thin-Film Transistors. *Nat. Mater.* **2006**, *5*, 222−228.

(10) Roy, I.; Hazra, S. Poor Solvent and Thermal Annealing Induced Ordered Crystallites in Poly(3-dodecylthiophene) Films. *RSC Adv.* **2015**, *5*, 665−675.

(11) Gargi, D.; Kline, R. J.; DeLongchamp, D. M.; Fischer, D. A.; Toney, M. F.; O'Connor, B. T. Charge Transport in Highly Face-on Poly(3-hexylthiophene) Films. *J. Phys. Chem. C* **2013**, *117*, 17421−17428.

(12) Chang, J.-F.; Sun, B.; Breiby, D. W.; Nielsen, M. M.; Sölling, T. I.; Giles, M.; McCulloch, I.; Sirringhaus, H. Enhanced Mobility of Poly(3-hexylthiophene) Transistors by Spin-coating from High-Boiling-Point Solvents. *Chem. Mater.* **2004**, *16*, 4772−4776.

(13) Clark, J.; Silva, C.; Friend, R. H.; Spano, F. C. Role of Intermolecular Coupling in the Photophysics of Disordered Organic Semiconductors: Aggregate Emission in Regioregular Polythiophene. *Phys. Rev. Lett.* **2007**, *98*, 206406.

(14) Bürgi, L.; Turbiez, M.; Pfeiffer, R.; Bienewald, F.; Kirner, H.; Winnewisser, C. High-Mobility Ambipolar Near-Infrared Light-Emitting Polymer Field-Effect Transistors. *Adv. Mater.* **2008**, *20*, 2217−2224.

(15) Zhou, E.; Yamakawa, S.; Tajima, K.; Yang, C.; Hashimoto, K. Synthesis and Photovoltaic Properties of Diketopyrrolopyrrole-based Donor−Acceptor Copolymers. *Chem. Mater.* **2009**, *21*, 4055−4061.

(16) Li, Y.; Sonar, P.; Murphy, L.; Hong, W. High Mobility Diketopyrrolopyrrole (DPP)-based Organic Semiconductor Materials for Organic Thin Film Transistors and Photovoltaics. *Energy Environ. Sci.* **2013**, *6*, 1684−1710.

(17) Kim, H. G.; Kang, B.; Ko, H.; Lee, J.; Shin, J.; Cho, K. Synthetic Tailoring of Solid-State Order in Diketopyrrolopyrrole-Based Copolymers via Intramolecular Noncovalent Interactions. *Chem. Mater.* **2015**, *27*, 829−838.

(18) Yoon, G. B.; Kwon, H.-Y.; Jung, S.-H.; Lee, J.-K.; Lee, J. Effect of Donor Building Blocks on the Charge-Transfer Characteristics of Diketopyrrolopyrrole-Based Donor−Acceptor-Type Semiconducting Copolymers. *ACS Appl. Mater. Interfaces* **2017**, *9*, 39502−39510.

(19) Tsao, H. N.; Cho, D.; Andreasen, J. W.; Rouhanipour, A.; Breiby, D. W.; Pisula, W.; Müllen, K. The Influence of Morphology

on High-Performance Polymer Field-Effect Transistors. *Adv. Mater.* **2009**, *21*, 209−212.
(20) Li, Y.; Singh, S. P.; Sonar, P. A High Mobility P-Type DPP-Thieno[3,2-b]thiophene Copolymer for Organic Thin-Film Transistors. *Adv. Mater.* **2010**, *22*, 4862−4866.
(21) Nahid, M. M.; Welford, A.; Gann, E.; Thomsen, L.; Sharma, K. P.; McNeill, C. R. Nature and Extent of Solution Aggregation Determines the Performance of P(NDI2OD-T2) Thin-Film Transistors. *Adv. Electron. Mater.* **2018**, *4*, 1700559.
(22) McCulloch, I.; Heeney, M.; Bailey, C.; Genevicius, K.; MacDonald, I.; Shkunov, M.; Sparrowe, D.; Tierney, S.; Wagner, R.; Zhang, W.; Chabinyc, M. L.; Kline, R. J.; McGehee, M. D.; Toney, M. F. Liquid-Crystalline Semiconducting Polymers with High Charge-Carrier Mobility. *Nat. Mater.* **2006**, *5*, 328−333.
(23) Pan, H.; Li, Y.; Wu, Y.; Liu, P.; Ong, B. S.; Zhu, S.; Xu, G. Low-Temperature, Solution-Processed, High-Mobility Polymer Semiconductors for Thin-Film Transistors. *J. Am. Chem. Soc.* **2007**, *129*, 4112−4113.
(24) Osaka, I.; Abe, T.; Shinamura, S.; Miyazaki, E.; Takimiya, K. High-Mobility Semiconducting Naphthodithiophene Copolymers. *J. Am. Chem. Soc.* **2010**, *132*, 5000−5001.
(25) Li, J.; Zhao, Y.; Tan, H. S.; Guo, Y.; Di, C.-A.; Yu, G.; Liu, Y.; Lin, M.; Lim, S. H.; Zhou, Y.; Su, H.; Ong, B. S. A Stable Solution-processed Polymer Semiconductor with Record High-mobility for Printed Transistors. *Sci. Rep.* **2012**, *2*, 754.
(26) Armin, A.; Wolfer, P.; Shaw, P. E.; Hambsch, M.; Maasoumi, F.; Ullah, M.; Gann, E.; McNeill, C. R.; Li, J.; Shi, Z.; Burn, P. L.; Meredith, P. Simultaneous Enhancement of Charge Generation Quantum Yield and Carrier Transport in Organic Solar Cells. *J. Mater. Chem. C* **2015**, *3*, 10799−10812.
(27) Mitzi, D. B.; Kosbar, L. L.; Murray, C. E.; Copel, M.; Afzali, A. High-Mobility Ultrathin Semiconducting Films Prepared by Spin Coating. *Nature* **2004**, *428*, 299−303.
(28) Tyona, M. A Theoritical Study on Spin Coating Technique. *Adv. Mater. Res.* **2013**, *2*, 195−208.
(29) Lee, G.-Y.; Han, A.-R.; Kim, T.; Lee, H. R.; Oh, J. H.; Park, T. Requirements for Forming Efficient 3-D Charge Transport Pathway in Diketopyrrolopyrrole-Based Copolymers: Film Morphology vs Molecular Packing. *ACS Appl. Mater. Interfaces* **2016**, *8*, 12307−12315.
(30) Son, S. Y.; Lee, G.-Y.; Kim, S.; Park, W.-T.; Park, S. A.; Noh, Y.-Y.; Park, T. Control of Crystallite Orientation in Diketopyrrolopyrrole-Based Semiconducting Polymers via Tuning of Intermolecular Interactions. *ACS Appl. Mater. Interfaces* **2019**, *11*, 10751−10757.
(31) Venkatesh, R.; Zheng, Y.; Viersen, C.; Liu, A.; Silva, C.; Grover, M.; Reichmanis, E. Data Science Guided Experiments Identify Conjugated Polymer Solution Concentration as a Key Parameter in Device Performance. *ACS Mater. Lett.* **2021**, *3*, 1321−1327.
(32) Venkatesh, R.; Zheng, Y.; Liu, A. L.; Zhao, H.; Silva, C.; Takacs, C. J.; Grover, M. A.; Meredith, J. C.; Reichmanis, E. Overlap Concentration Generates Optimum Device Performance for DPP-based Conjugated Polymers. *Org. Electron.* **2023**, *117*, 106779.
(33) Choi, D.; Jin, S.; Lee, Y.; Kim, S. H.; Chung, D. S.; Hong, K.; Yang, C.; Jung, J.; Kim, J. K.; Ree, M.; et al. Direct Observation of Interfacial Morphology in Poly(3-hexylthiophene) Transistors: Relationship between Grain Boundary and Field-Effect Mobility. *ACS Appl. Mater. Interfaces* **2010**, *2*, 48−53.
(34) Parratt, L. G. Surface Studies of Solids by Total Reflection of X-rays. *Phys. Rev.* **1954**, *95*, 359−369.
(35) Tolan, M. *X-ray Scattering from Soft-Matter Thin Films: Materials Science and Basic Research*; Springer, 1999.
(36) Gibaud, A.; Hazra, S. X-ray Reflectivity and Diffuse Scattering. *Curr. Sci.* **2000**, *78*, 1467−1477.
(37) Daillant, J.; Gibaud, A. *X-ray and Neutron Reflectivity: Principles and Applications*; Springer, 2008.
(38) Bal, J.; Hazra, S. Interfacial Role in Room-Temperature Diffusion of Au into Si Substrates. *Phys. Rev. B: Condens. Matter Mater. Phys.* **2007**, *75*, 205411.
(39) Chatterjee, P.; Hazra, S.; Amenitsch, H. Substrate and Drying Effect in Shape and Ordering of Micelles Inside CTAB−Silica Mesostructured Films. *Soft Matter* **2012**, *8*, 2956−2964.
(40) Saifuddin, M.; Mukhopadhyay, M.; Biswas, A.; Gigli, L.; Plaisier, J. R.; Hazra, S. Tuning the Edge-on Oriented Ordering of Solution-Aged Poly(3-hexylthiophene) Thin Films. *J. Mater. Chem. C* **2020**, *8*, 8804−8813.
(41) Bal, J.; Hazra, S. Time-Evolution Growth of Ag Nanolayers on Differently-Passivated Si(001) Surfaces. *Phys. Rev. B: Condens. Matter Mater. Phys.* **2009**, *79*, 155412.
(42) Chatterjee, P.; Hazra, S. Time Evolution of a Cl-Terminated Si Surface at Ambient Conditions. *J. Phys. Chem. C* **2014**, *118*, 11350−11356.
(43) Mukhopadhyay, M.; Hazra, S. Interfacial and Thermal Energy Driven Growth and Evolution of Langmuir−Schaefer Monolayers of Au-Nanoparticles. *Phys. Chem. Chem. Phys.* **2018**, *20*, 1051−1062.
(44) Roy, S.; Saifuddin, M.; Mandal, S.; Hazra, S. Stearic Acid Mediated Growth of Edge-on Oriented Bilayer Poly(3-hexylthiophene) Langmuir Films. *J. Colloid Interface Sci.* **2022**, *606*, 1153−1162.
(45) Spano, F. C. Modeling Disorder in Polymer Aggregates: The Optical Spectroscopy of Regioregular Poly(3-hexylthiophene) Thin Films. *J. Chem. Phys.* **2005**, *122*, 234701.
(46) Spano, F. C. The Spectral Signatures of Frenkel Polarons in H- and J-Aggregates. *Acc. Chem. Res.* **2010**, *43*, 429−439.
(47) Hestand, N. J.; Spano, F. C. Expanded Theory of H- and J-Molecular Aggregates: The Effects of Vibronic Coupling and Intermolecular Charge Transfer. *Chem. Rev.* **2018**, *118*, 7069−7163.
(48) Saifuddin, M.; Roy, S.; Mandal, S.; Hazra, S. Vibronic States and Edge-On Oriented π-Stacking in Poly(3-alkylthiophene) Thin Films. *ACS Appl. Polym. Mater.* **2022**, *4*, 1377−1386.
(49) Ahmed, I.; Dildar, L.; Haque, A.; Patra, P.; Mukhopadhyay, M.; Hazra, S.; Kulkarni, M.; Thomas, S.; Plaisier, J. R.; Dutta, S. B.; Bal, J. K. Chitosan−Fatty Acid Interaction Mediated Growth of Langmuir Monolayer and Langmuir-Blodgett Films. *J. Colloid Interface Sci.* **2018**, *514*, 433−442.
(50) Mahato, S.; Puigdollers, J.; Voz, C.; Mukhopadhyay, M.; Mukherjee, M.; Hazra, S. Near 5% DMSO is the Best: A Structural Investigation of PEDOT:PSS Thin Films with Strong Emphasis on Surface and Interface for Hybrid Solar Cell. *Appl. Surf. Sci.* **2020**, *499*, 143967.
(51) Zhong, W.; Sun, S.; Ying, L.; Liu, F.; Lan, L.; Huang, F.; Cao, Y. High-Performance Organic Field-Effect Transistors Fabricated Based on a Novel Ternary π-Conjugated Copolymer. *ACS Appl. Mater. Interfaces* **2017**, *9*, 7315−7321.
(52) Yu, K.; Park, B.; Kim, G.; Kim, C. H.; Park, S.; Kim, J.; Jung, S.; Jeong, S.; Kwon, S.; Kang, H.; et al. Optically Transparent Semiconducting Polymer Nanonetwork for Flexible and Transparent Electronics. *Proc. Natl. Acad. Sci. U.S.A.* **2016**, *113*, 14261−14266.
(53) Xu, Z.; Park, K. S.; Kwok, J. J.; Lin, O.; Patel, B. B.; Kafle, P.; Davies, D. W.; Chen, Q.; Diao, Y. Not All Aggregates Are Made the Same: Distinct Structures of Solution Aggregates Drastically Modulate Assembly Pathways, Morphology, and Electronic Properties of Conjugated Polymers. *Adv. Mater.* **2022**, *34*, 2203055.
(54) Yamagata, H.; Hestand, N. J.; Spano, F. C.; Köhler, A.; Scharsich, C.; Hoffmann, S. T.; Bässler, H. The Red-Phase of Poly[2-methoxy-5-(2-ethylhexyloxy)-1, 4-phenylenevinylene](MEH-PPV): A Disordered HJ-Aggregate. *J. Chem. Phys.* **2013**, *139*, 114903.
(55) Yu, S. H.; Park, K. H.; Kim, Y.-H.; Chung, D. S.; Kwon, S.-K. Fine Molecular Tuning of Diketopyrrolopyrrole-based Polymer Semiconductors for Efficient Charge Transport: Effects of Intramolecular Conjugation Structure. *Macromolecules* **2017**, *50*, 4227−4234.
(56) Hidayat, A. T.; Benten, H.; Ohta, N.; Na, Y.; Muraoka, A.; Kojima, H.; Jung, M.-C.; Nakamura, M. Enhancement of Short-Range Ordering of Low-Bandgap Donor−Acceptor Conjugated Polymer in Polymer/Polymer Blend Films. *Macromolecules* **2020**, *53*, 6630−6639.
(57) Chandran, S.; Baschnagel, J.; Cangialosi, D.; Fukao, K.; Glynos, E.; Janssen, L. M.; Müller, M.; Muthukumar, M.; Steiner, U.; Xu, J.;

https://doi.org/10.1021/acs.macromol.3c00885
Macromolecules 2023, 56, 7065−7077

Napolitano, S.; Reiter, G. Processing Pathways Decide Polymer Properties at the Molecular Level. *Macromolecules* **2019**, *52*, 7146−7156.
(58) Kiessig, H. Interferenz von Röntgenstrahlen an dünnen Schichten. *Ann. Phys.* **1931**, *402*, 769−788.
(59) Roy, I.; Hazra, S. Structures of Spin-Coated and Annealed Monolayer and Multilayer Poly(3-dodecylthiophene) Thin Films. *RSC Adv.* **2017**, *7*, 2563−2572.
(60) Roy, I.; Hazra, S. Solvent Dependent Ordering of Poly(3-dodecylthiophene) in Thin Films. *Soft Matter* **2015**, *11*, 3724−3732.
(61) Mukhopadhyay, M.; Hazra, S. Growth of Thiol-Coated Au-Nanoparticle Langmuir Monolayers Through a 2D-network of Disk-like Islands. *RSC Adv.* **2016**, *6*, 12326−12336.
(62) Yabuuchi, Y.; Minowa, Y.; Nagamatsu, S.; Fujii, A.; Ozaki, M. Dynamics of Preaggregation and Film Formation of Donor−Acceptor π-Conjugated Polymers. *ACS Mater. Lett.* **2022**, *4*, 205−211.
(63) Yun, H. S.; Kim, D. H.; Kwon, H. G.; Choi, H. K. Centrifugal Force-Induced Alignment in the Self-Assembly of Block Copolymers. *Macromolecules* **2022**, *55*, 4305−4312.
(64) Klauk, H. Organic Thin-Film Transistors. *Chem. Soc. Rev.* **2010**, *39*, 2643−2666.
(65) Salleo, A. Charge Transport in Polymeric Transistors. *Mater. Today* **2007**, *10*, 38−45.
(66) Salleo, A.; Kline, R. J.; DeLongchamp, D. M.; Chabinyc, M. L. Microstructural Characterization and Charge Transport in Thin Films of Conjugated Polymers. *Adv. Mater.* **2010**, *22*, 3812−3838.

https://doi.org/10.1021/acs.macromol.3c00885
Macromolecules 2023, 56, 7065−7077